PERGAMON

Journal of Quantitative Spectroscopy & Radiative Transfer 62 (1999) 279–302

Journal of Quantitative Spectroscopy & Radiative Transfer

Non-grey benchmark results for two temperature non-equilibrium radiative transfer

Bingjing Su[a,*], Gordon L. Olson[b]

[a] *Department of Mechanical, Industrial and Nuclear Engineering, University of Cincinnati, Cincinnati, OH 45221-0072, USA*

[b] *Los Alamos National Laboratory, Transport Methods Group, Los Alamos, NM 87545, USA*

Received 13 August 1998

Abstract

Benchmark solutions to time-dependent radiative transfer problems involving non-equilibrium coupling to the material temperature field are crucial for validating time-dependent radiation transport codes. Previous efforts on generating analytical solutions to non-equilibrium radiative transfer problems were all restricted to the one-group grey model. In this paper, a non-grey model, namely the picket-fence model, is considered for a two temperature non-equilibrium radiative transfer problem in an infinite medium. The analytical solutions, as functions of space and time, are constructed in the form of infinite integrals for both the diffusion description and transport description. These expressions are evaluated numerically and the benchmark results are generated. The asymptotic solutions for large and small times are also derived in terms of elementary functions and are compared with the exact results. Comparisons are given between the transport and diffusion solutions and between the grey and non-grey solutions. © 1999 Elsevier Science Ltd. All rights reserved.

1. Introduction

Time-dependent radiative transfer problems with the radiation and material energy fields in non-equilibrium are generally very complex and have to be solved numerically. Many computer codes for these types of problems, employing different numerical algorithms and techniques, exist in the engineering and scientific community. In order to verify the numerical procedures used in codes and assess the accuracies of codes, it is often desirable to have analytical benchmarks for some reference problems, to which numerical solutions (code results) can be compared. In the

* Corresponding author. Tel.: + 1 513 556 2960; fax: + 1 513 556 3390; e-mail: bingjing.su@uc.edu

0022-4073/99/$ - see front matter © 1999 Elsevier Science Ltd. All rights reserved.
PII: S0022-4073(98)00105-8

context used here, an analytical benchmark means a closed-form representation to a radiative transfer problem for which an accurate numerical evaluation can be performed.

Some analytical benchmarks for time-dependent and non-equilibrium radiative transfer problems exist in the literature. Particularly, the non-equilibrium Marshak wave problem [1], where an initially cold, semi-infinite, purely absorbing, and homogeneous medium is irradiated isotropically at the free surface, has received considerable attention. The full Marshak wave problem is non-linear and is, therefore, mathematically intractable. But with several simplifying assumptions on material properties [2], it has been linearized and thus analyzed. Specifically, this problem has been considered in the diffusion and low-order spherical harmonic (P_1 and P_2) approximations, and the analytic solutions were obtained for the radiation density and material temperature at the free surface and for the spatially integrated radiation and material energy contents as functions of time [2, 3], as well as for the full radiation and material temperature fields in the interior of the medium as functions of space and time [2, 4]. In the transport description, Ganapol and Pomraning [5] solved the problem using a multiple-collision approach and gave the transport solutions for the radiation density and material temperature at the free surface and for the radiation and material energy contents. No transport solution for the distribution of radiation and material temperature in the medium was given in that paper [5]. Later in an unpublished report, Ganapol [6] closed the gap and derived the transport solution in the interior of medium. However, only figures showing space-time solutions were presented and no tabulated numerical results were available for the interior of medium. In order to generate a detailed numerical benchmark for full space-time transport solution in the interior of medium and also partially due to their unfamiliarity with the multiple collision approach, Su and Olson [7] considered a different and mathematically simpler non-equilibrium radiative transfer problem than the foregoing Marshak wave problem. For this new problem the full solutions, as functions of space and time, were constructed easily for radiation and material energy fields in a straightforward way and detailed numerical results were given.

All the above analytical benchmarks were generated for the one-group grey model. That is, there is no frequency dependence in the problems. However, in reality some of the material properties, such as the opacity, varies by orders of magnitude over the frequency structure and the frequency variable is almost universally treated by the multigroup method. Obviously, there is a need to have non-grey benchmarks to test codes in more detail. In this paper, we reconsider the same problem considered earlier in Ref. [7] by using a non-grey model, namely the picket-fence model. In this model, the frequency variable is divided into two (or more) groups. So, this work is an extension of Ref. [7] to include the frequency variable. In the next section, we describe the problem and the picket-fence model for completeness. The general solutions, asymptotic solutions and numerical results to the problem are given in Section 3 for the diffusion description and in Section 4 for the transport description, respectively. In Section 5, comparisons between the diffusion and transport solutions and between the two-group picket-fence model and the one-group grey model are presented. Some concluding remarks are given in the last section.

2. The problem and the picket-fence model

We consider a basic non-equilibrium radiative transfer problem, which corresponds to an initially cold, homogeneous, infinite, and purely absorbing medium with an internal isotropic

radiation source. Hydrodynamic motion and heat conduction are assumed unimportant and thus neglected. For a general temperature dependence of the material properties, the equations describing this problem are non-linear and thus analytically intractable. As shown previously [2–7], these equations become linear in the radiation intensity and the fourth power of the material temperature if the opacity (absorption cross section) is taken as independent of temperature, and the material specific heat is assumed proportional to the cube of the material temperature. It should be pointed out that the sole purpose of these assumptions on material properties is to relax the physical content of the problem such that a detailed analytic solution can be obtained and thus provide a useful test problem for radiative transfer codes, since those codes are meant to handle an arbitrary temperature dependence of the material properties. With these assumptions, the coupled radiation transport and material balance equations in one dimensional plane geometry for this problem, including the frequency variable, are given by

$$\frac{1}{c}\frac{\partial I}{\partial t}+\mu\frac{\partial I}{\partial z}=\kappa\,(B-I)+\frac{S}{4\pi}, \tag{1}$$

$$\frac{\alpha}{4}\frac{\partial T^4}{\partial t}=2\pi\int_{-1}^{1}\mathrm{d}\mu\int_{0}^{\infty}\mathrm{d}\nu\,\kappa\,(I-B). \tag{2}$$

Here, z and t are the spatial and temporal coordinates; μ is the cosine of the photon direction measured with respect to the z axis; ν is the frequency variable; $I(z, \nu, \mu, t)$ is the radiative intensity; $T(z, t)$ is the material temperature; $B[\nu, T(z, t)]$ is the Planck function; $S(z, \nu, t)$ is the interior radiation source; $\kappa(\nu)$ is the opacity of material and could be a strong function of ν; α is the proportionality constant for the cube temperature dependence of the specific heat; and c is the speed of light. The boundary and initial conditions on Eqs. (1) and (2) are

$$\lim_{z\to\pm\infty} I(z, \nu, \mu, t)=I(z, \nu, \mu, 0)=T(z, 0)=0. \tag{3}$$

We take the opacity $\kappa(\nu)$ to be given by the two-value (or more general n-value) picket-fence model, which is defined as follows. Consider a small frequency interval $\Delta\nu$ at some frequency ν. This interval is small enough (essentially differential in size) so that the Planck function $B(\nu,T)$ and the external source $S(z, \nu, t)$ can be assumed not to vary over $\Delta\nu$. At any frequency within $\Delta\nu$, the opacity assumes one of the two values, which we denote by κ_n, $n=1, 2$. We let p_n be the fraction of the interval $\Delta\nu$ for which the opacity is κ_n, and assume that the p_n are independent of ν. That is, the p_n are independent of where $\Delta\nu$ is placed on the spectrum $0\le\nu<\infty$. Certainly, we have $p_1+p_2=1$ and we define an averaged opacity $\bar{\kappa}$ as

$$\bar{\kappa}=p_1\kappa_1+p_2\kappa_2\,, \tag{4}$$

which defines a natural length scale for the problem.

We next let ν_n denote all values of ν on the interval $0\le\nu<\infty$ for which $\kappa(\nu)=\kappa_n$. If we integrate Eq. (1) over ν_n, define

$$I_n(z, \mu, t)=\int_{\nu_n}\mathrm{d}\nu\, I(z, \nu, \mu, t), \tag{5}$$

and use

$$\int_0^\infty \mathrm{d}\nu\, B(\nu, T) = \frac{acT^4}{4\pi}, \tag{6}$$

$$\int_0^\infty \mathrm{d}\nu\, S(z, \nu, t) = S_0(z, t), \tag{7}$$

then Eqs. (1) and (2) become

$$\frac{1}{c}\frac{\partial I_n}{\partial t} + \mu\frac{\partial I_n}{\partial z} = \kappa_n\left[p_n\frac{acT^4}{4\pi} - I_n\right] + p_n\frac{S_0}{4\pi}, \quad n = 1, 2, \tag{8}$$

$$\frac{\alpha}{4}\frac{\partial T^4}{\partial t} = 2\pi\sum_{n=1}^{2}\kappa_n\int_{-1}^{1}\mathrm{d}\mu\, I_n - \bar{\kappa}acT^4. \tag{9}$$

The parameter a in the above equations is the radiation constant. As in the previous work [2–7], we rewrite Eqs. (8) and (9) in the form of dimensionless variables given by

$$\varepsilon\frac{\partial u_n}{\partial \tau} + \mu\frac{\partial u_n}{\partial x} = w_n\left[\frac{p_n V}{2} - u_n\right] + p_n\frac{Q}{2}, \quad n = 1, 2, \tag{10}$$

$$\frac{\partial V}{\partial \tau} = \sum_{n=1}^{2} w_n\int_{-1}^{1}\mathrm{d}\mu\, u_n - V, \tag{11}$$

where $x \equiv \bar{\kappa}z$, $w_n \equiv \kappa_n/\bar{\kappa}$, $\varepsilon \equiv 4a/\alpha$, $\tau \equiv \varepsilon c\bar{\kappa}t$, $u_n(x, \mu, \tau) \equiv 2\pi I_n(z, \mu, t)/(acT_0^4)$, $V(x, \tau) \equiv [T(z, t)/T_0]^4$, and $Q(x, \tau) \equiv S_0(z, t)/(ac\bar{\kappa}T_0^4)$, with T_0 being a reference temperature. In these new variables, x and τ are the scaled spatial and temporal variables, and u_n, V, and Q are the dimensionless radiation intensity, material energy density, and radiation source, respectively. The material properties are now represented by w_n, with $p_1w_1 + p_2w_2 = 1$, and ε.

The boundary and initial conditions for Eqs. (10) and (11) are,

$$\lim_{x\to\pm\infty} u_n(x, \mu, \tau) = u_n(x, \mu, 0) = V(x, 0) = 0\,. \tag{12}$$

These conditions imply that the material is initially cold and suffers no irradiation before the interior source $Q(x, \tau)$ is turned on at $\tau = 0$. We specify Q to be a unit radiation source which is constant in time but only exists in a finite period of time ($0 \le \tau \le \tau_0$) and is uniformly distributed in a finite space ($-x_0 \le x \le x_0$), i.e.

$$Q(x, \tau) = Q_1(x)Q_2(\tau) \tag{13}$$

with

$$Q_1(x) = \frac{1}{2x_0}[\theta(x + x_0) - \theta(x - x_0)]\,, \tag{14}$$

$$Q_2(\tau) = \theta(\tau) - \theta(\tau - \tau_0)\,. \tag{15}$$

The θ in Eqs. (14) and (15) is the Heaviside (unit step) function. The mathematical objective for Eqs. (10)–(15) is to derive the analytic expressions for u_n and V so that very accurate numerical results can be generated.

3. Solutions to the diffusion description

Diffusion theory is still used in radiative transfer calculations, because it can yield approximate solutions very quickly. In this section, we generate the benchmark results for diffusion theory. The diffusion description for the problem we just discussed is given by

$$\varepsilon \frac{\partial U_n}{\partial \tau} - \frac{1}{3w_n} \frac{\partial^2 U_n}{\partial x^2} = w_n(p_n V - U_n) + p_n Q, \quad n = 1, 2, \tag{16}$$

$$\frac{\partial V}{\partial \tau} = \sum_{n=1}^{2} w_n U_n - V, \tag{17}$$

$$\lim_{x \to \pm \infty} U_n(x, \tau) = U_n(x, 0) = V(x, 0) = 0, \tag{18}$$

where U_n is the scalar radiation energy density defined by

$$U_n(x, \tau) = \int_{-1}^{1} \mathrm{d}\mu \, u_n(x, \mu, \tau). \tag{19}$$

3.1. The general solutions

To solve Eqs. (16)–(18), we apply the Fourier transform with respect to the spatial variable x and apply the Laplace transform with respect to the temporal variable τ. That is, we introduce the double transforms according to

$$\bar{f}(k, s) = \int_0^{\infty} \mathrm{d}\tau \, \mathrm{e}^{-s\tau} \int_{-\infty}^{\infty} \mathrm{d}x \, \mathrm{e}^{-\mathrm{i}kx} f(x, \tau). \tag{20}$$

After the transformations, Eqs. (16) and (17) become coupled linear algebraic equations for $\bar{U}_n$ and $\bar{V}$. Solving these algebraic equations, we have

$$\bar{U}_n = p_n \bar{Q}(k, s) \frac{\varepsilon s^2 + [\varepsilon + w_m + k^2/(3w_m)]s + w_1 w_2 + k^2/(3w_m)}{\varepsilon^2 s^3 + b_2 s^2 + b_1 s + b_0},$$

$$n, m = 1, 2, m \neq n, \tag{21}$$

$$\bar{V} = \bar{Q}(k, s) \frac{\varepsilon s + w_1 w_2 + (p_1 w_1^2 + p_2 w_2^2)k^2/(3w_1 w_2)}{\varepsilon^2 s^3 + b_2 s^2 + b_1 s + b_0}, \tag{22}$$

where

$$\bar{Q}(k, s) = \bar{Q}_1(k) \bar{Q}_2(s) \tag{23}$$

with

$$\bar{Q}_1(k) = \frac{\sin(kx_0)}{kx_0}, \tag{24}$$

$$\bar{Q}_2(s) = \frac{1 - e^{-\tau_0 s}}{s}, \tag{25}$$

and

$$b_2 = \varepsilon(w_1 + w_2 + \varepsilon) + \frac{\varepsilon(w_1 + w_2)k^2}{3w_1w_2}, \tag{26}$$

$$b_1 = w_1w_2(1 + \varepsilon) + \frac{(w_1^2 + w_2^2 + \varepsilon w_1 + \varepsilon w_2)k^2}{3w_1w_2} + \frac{k^4}{9w_1w_2}, \tag{27}$$

$$b_0 = \frac{1}{3}(p_1w_2 + p_2w_1)k^2 + \frac{k^4}{9w_1w_2}. \tag{28}$$

The solutions $U_n(x, \tau)$ and $V(x, \tau)$ follow from the double inversions of Eqs. (21) and (22). To proceed, we rewrite the denominator of Eqs. (21) and (22) as

$$\varepsilon^2 s^3 + b_2 s^2 + b_1 s + b_0 = \varepsilon^2(s + s_1)(s + s_2)(s + s_3). \tag{29}$$

The s_j ($j = 1 - 3$), which all turn out to be real, are found by the Cardano's formula [8] and given by

$$s_1 = \frac{b_2}{3\varepsilon^2} - 2R\cos(\theta/3), \tag{30}$$

$$s_2 = \frac{b_2}{3\varepsilon^2} + R[\cos(\theta/3) - \sqrt{3}\sin(\theta/3)], \tag{31}$$

$$s_3 = \frac{b_2}{3\varepsilon^2} + R[\cos(\theta/3) + \sqrt{3}\sin(\theta/3)], \tag{32}$$

where

$$R = \sqrt[6]{\frac{q^2}{4} + g}, \tag{33}$$

$$\theta = \tan^{-1}\left(\frac{2\sqrt{g}}{q}\right) + \begin{cases} \pi, & q < 0, \\ 0, & q \geq 0, \end{cases} \tag{34}$$

$$q = -\frac{b_0}{\varepsilon^2} + \frac{b_1b_2}{3\varepsilon^4} - \frac{2b_2^3}{27\varepsilon^6}, \tag{35}$$

$$g = \frac{1}{27}\left(\frac{b_2^2}{3\varepsilon^4} - \frac{b_1}{\varepsilon^2}\right)^3 - \frac{q^2}{4}. \tag{36}$$

The g given by Eq. (36) is positive for all k.

With the s_j known, we rearrange $\bar{U}_n$ and $\bar{V}$, denoted here by $\bar{W}$ in general, as

$$\bar{W}(k,s) = \bar{Q}_1(k)\bar{Q}_2(s)\sum_{j=1}^{3}\frac{A_j(k)}{s+s_j(k)}. \tag{37}$$

The coefficients $A_j(k)$ are given by

$$A_j(k) = \frac{N(-s_j)}{D'(-s_j)}, \tag{38}$$

where N represents the numerator and D' represents the first derivative, with respect to s, of the denominator of $\bar{U}_n$ or $\bar{V}$. The Laplace inversion of Eq. (37) can be done analytically and yields

$$\bar{W}(k,\tau) = \bar{Q}_1(k)\sum_{j=1}^{3}\frac{A_j}{s_j}(\mathrm{e}^{-s_j\tau^*} - \mathrm{e}^{-s_j\tau}), \tag{39}$$

where

$$\tau^* = \max[0,(\tau-\tau_0)]. \tag{40}$$

However, the Fourier inversion of Eq. (39) has to be performed numerically due to the complex dependence of A_j and s_j on k. Using the inversion formula and the fact that all s_j and A_j are symmetric in k, we finally have

$$W(x,\tau) = \frac{1}{\pi}\int_0^\infty \mathrm{d}k\cos(kx)\bar{Q}_1(k)\sum_{j=1}^{3}\frac{A_j}{s_j}(\mathrm{e}^{-s_j\tau^*} - \mathrm{e}^{-s_j\tau}), \tag{41}$$

which is the general solution representation for $U_1(x,\tau)$, $U_2(x,\tau)$, and $V(x,\tau)$, with A_j determined individually for each quantity.

3.2. The asymptotic solutions

The exact solutions for U_n and V come from the inverse transformations of Eqs. (21) and (22). As just shown, the complete inversion cannot be performed analytically and some numerical work is required in this process. However, the asymptotic solutions at large times and small times are available in elementary functions. The details of these asymptotic analyses is analogous to that given in Ref. [7]. Here we only outline the main steps and give the results without too much algebraic detail.

It is easy to verify that the roots s_j monotonically increase with k, with $s_3 > s_2 > s_1 > 0$. According to Eq. (41), the main contribution to the solutions, at large times ($\tau \gg \tau_0$), comes from small k and s_1. To obtain simple asymptotic solutions at large times, we neglect the contributions from s_2 and s_3. Since at large times the main contribution to the Laplace inversion is due to small s, we assume

$$\varepsilon^2 s^3 \ll b_2 s^2 \ll b_1 s \ll b_0, \tag{42}$$

neglect the quadratic and cubic terms of s correspondingly in Eq. (29), and approximate s_1 by b_0/b_1 for small s. Expanding s_1, $\bar{Q}_1$, and $\bar{Q}_2$ at small k and small s as

$$s_1 \approx \frac{\alpha_1}{3(1+\varepsilon)}k^2, \tag{43}$$

$$\bar{Q}_1(k) \approx 1 - \tfrac{1}{3}x_0^2k^2, \tag{44}$$

$$\bar{Q}_2(s) \approx \tau_0(1 - \tfrac{1}{2}\tau_0 s), \tag{45}$$

finding A_1 and expanding it at $k = 0$ up to the quadratic term in k, we obtain an approximation to Eq. (37) at small s and small k. Converting these simplified $\bar{U}_n$ and $\bar{V}$ back to the $x - \tau$ domain analytically yields the following asymptotic solutions at large times given by

$$U_n(x,\tau) = p_n\frac{\tau_0}{2}\sqrt{\frac{3}{\alpha_1\pi(1+\varepsilon)\tau}}\left[1 + \frac{\beta_n}{2\alpha_1\tau} - \frac{3\beta_n(1+\varepsilon)x^2}{4\alpha_1^2\tau^2}\right]\exp\left[-\frac{3(1+\varepsilon)x^2}{4\alpha_1\tau}\right], \tag{46}$$

$$V(x,\tau) = \frac{\tau_0}{2}\sqrt{\frac{3}{\alpha_1\pi(1+\varepsilon)\tau}}\left[1 + \frac{\beta_v}{2\alpha_1\tau} - \frac{3\beta_v(1+\varepsilon)x^2}{4\alpha_1^2\tau^2}\right]\exp\left[-\frac{3(1+\varepsilon)x^2}{4\alpha_1\tau}\right], \tag{47}$$

where

$$\beta_n = \frac{\alpha_1\tau_0}{2} - (1+\varepsilon)x_0^2 + \frac{2\varepsilon}{1+\varepsilon}\alpha_1^2 + \frac{\varepsilon - w_m}{w_1w_2}\alpha_1 - \alpha_2 - \frac{1+\varepsilon-w_n}{w_n^2w_m},$$

$$n, m = 1, 2, m \neq n, \tag{48}$$

$$\beta_v = \frac{\alpha_1\tau_0}{2} - (1+\varepsilon)x_0^2 + \frac{2\varepsilon\alpha_1^2}{1+\varepsilon} + \frac{\varepsilon(\alpha_1 - 1)}{w_1w_2} - \alpha_2\,. \tag{49}$$

The α_1 and α_2 in these equations are defined by

$$\alpha_1 = \frac{p_1}{w_1} + \frac{p_2}{w_2} = \frac{w_1 + w_2 - 1}{w_1w_2}, \tag{50}$$

$$\alpha_2 = \frac{p_1}{w_1^2} + \frac{p_2}{w_2^2} = \frac{w_1^2 + w_1w_2 + w_2^2 - w_1 - w_2}{w_1^2w_2^2}. \tag{51}$$

Small τ solutions are dominated by large values of s. Therefore, to obtain small τ asymptotic solutions, we assume

$$b_0 \ll b_1 s \ll b_2 s^2 \ll \varepsilon^2 s^3\,, \tag{52}$$

keep $\bar{Q}$ untouched, and expand the other parts of $\bar{U}_n$ and $\bar{V}$ into polynomials in terms of $1/s$. Keeping the terms up to $1/s^3$ and converting the resulting large s approximations for Eqs. (21) and (22) back to the $x - \tau$ domain, we obtain the asymptotic solutions for small times given by

$$U_n(x,\tau) = p_nQ_1(x)\left[\frac{\tau}{\varepsilon} - \frac{w_n\tau^2}{2\varepsilon^2} + \frac{w_n(w_n+\varepsilon)\tau^3}{6\varepsilon^3}\right], \tag{53}$$

$$V(x,\tau) = Q_1(x)\left[\frac{\tau^2}{2\varepsilon} - \frac{\tau^3}{6\varepsilon^2}(\varepsilon + w_1 + w_2 - w_1w_2)\right]. \tag{54}$$

As pointed out earlier [7], these small τ asymptotic solutions indicate that at very small times, the radiation and material energy densities only depend upon the local source. The effect of streaming (propagation of radiation) is totally neglected. This is justifiable for spatial positions well within the source region, where the spatial gradients of densities are very small. However, this is not the case near the edges of the source region (note that the source is uniformly distributed in $-x_0 \le x \le x_0$), where the spatial gradients of densities are huge and thus the effect of streaming is important. Therefore, Eqs. (53) and (54) are not valid near $\pm x_0$.

3.3. The numerical results

The benchmark results of $U_n(x,\tau)$ and $V(x,\tau)$ for the diffusion description are computed according to Eq. (41), with the integral being evaluated numerically. The whole integration range $(0 \le k \le \infty)$ is divided into subranges, i.e. we rewrite Eq. (41) as

$$W(x,\tau) = \frac{1}{\pi} \sum_{l=0}^{\infty} \int_{k_l}^{k_{l+1}} \mathrm{d}k \cos(kx) \bar{Q}_1(k) \sum_{j=1}^{3} \frac{A_j}{s_j} (\mathrm{e}^{-s_j\tau^*} - \mathrm{e}^{-s_j\tau}), \tag{55}$$

where k_l is defined as $l^2 2\pi/(x + x_0)$. For each subrange, $k_l \le k \le k_{l+1}$, the integral is evaluated by the Simpson's rule, i.e. each integration subrange is divided into 2^N equal intervals and N is successively increased from $N = 1, 2, 3, \ldots$, until a desired accuracy is achieved. We require the numerical results of $U_n(x,\tau)$ and $V(x,\tau)$ to have five digits after the decimal point; therefore, the convergence criteria is set to be 0.0001%. Specifically, the integral for each subrange is thought to be converged when a relative error of 0.0001% is achieved between two successive numerical evaluations (with halved intervals). The computation continues subrange by subrange until a subrange in which the absolute value of the integral is less than 1×10^{-7} is reached. This value (1×10^{-7}) is selected so that the neglected subranges contribute nothing to the total integration within the accuracy requirement (1×10^{-5}). As we have mentioned, the roots s_j increase monotonically with k. Thus, large k contribute little or nothing to the integral, especially at large times. Computations show that for most of (x, τ) points, the integral converges within first few subranges.

Three cases are chosen to be calculated. The parameters specifying the medium and the source are given in Table 1 for the three cases. Except for the group opacities w_1 and w_2, all the other parameters are the same for all the cases. For Case $\mathscr{A}$, we set $w_1 = w_2 = 1$ so that the two-group picket-fence model we are considering in this work is equivalent to the grey model we considered earlier [7]. We use this case as a test to check the algebraic manipulations and numerical methods involved in this work, since the grey solution [7] and the picket-fence model solution are

Table 1
Specification for the three cases

Case	x_0	τ_0	ε	p_1	p_2	w_1	w_2	w_2/w_1
$\mathscr{A}$	0.50	10.0	1.0	0.50	0.50	1	1	1
$\mathscr{B}$	0.50	10.0	1.0	0.50	0.50	2/11	20/11	10
$\mathscr{C}$	0.50	10.0	1.0	0.50	0.50	2/101	200/101	100

constructed differently. Calculations show that we do reproduce the grey model results by Eq. (55) for this case, as it should. This agreement gives us confidence on both of the treatments given here and in Ref. [7]. For Case $\mathscr{B}$, the ratio of the two opacities, w_2/w_1, is set to be 10; and for Case $\mathscr{C}$ that ratio is 100. These two non-grey cases are what we really are interested in.

To further test the numerical scheme, we compare the numerical results with the large τ and small τ asymptotic solutions for the three cases at $x = 0.1$. The results are given in Fig. 1. The quantity shown in the figure, D, is the relative error between asymptotic and numerical solutions and is defined as

$$D = \left| \frac{U_{\text{numerical}} - U_{\text{asymptotic}}}{U_{\text{numerical}}} \right|, \tag{56}$$

where $U(x, \tau) = U_1(x, \tau) + U_2(x, \tau)$ is the total radiation energy density. We see that the agreement between the numerical solutions and the both asymptotic solutions is very good for Case $\mathscr{A}$. Even at moderate small and moderate large τ, the relative errors are below 1%. However, for the same τ the agreement deteriorates for Case $\mathscr{B}$ and Case $\mathscr{C}$, where the ratio of w_2/w_1 becomes larger and larger. This phenomenon is not surprising. Because in our asymptotic analyses, we treated b_2, b_1, and b_0 given by Eqs. (26)–(28) as finite. Thus, in large τ (small s) analysis, we assumed and used Eq. (42); and in small τ (large s) analysis, we assumed and used Eq. (52). But, as w_2/w_1 goes to infinity (or equivalently as w_1 goes to zero due to the scaling of $p_1w_1 + p_2w_2 = 1$), b_0 through b_2 go to infinity too for non-zero k. As a result, the assumptions given by Eqs. (42) and (52) are compromised for very large values of w_2/w_1 and the asymptotic solutions obtained in Section 3.2 only work well at extremely small or extremely large τ for such cases, as suggested in the figure. Nevertheless, Fig. 1 clearly shows that the numerical results match the asymptotic solutions where

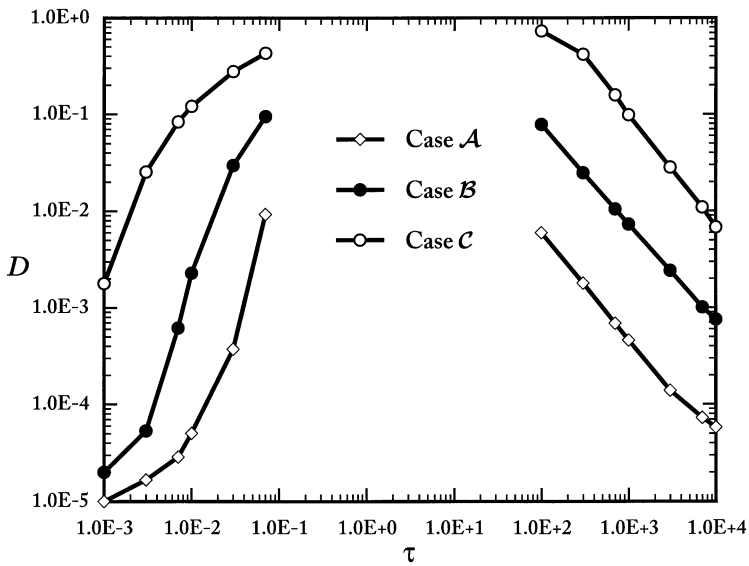

Fig. 1. Comparison between the numerical and asymptotic diffusion solutions.

they are appropriate and as τ goes to infinitely small or infinitely large the two solutions converge. Thus, the numerical scheme is validated at least to some extent.

The benchmark results for $U_1(x, \tau)$, $U_2(x, \tau)$, and $V(x, \tau)$, computed from Eq. (55), are given at selected $x - \tau$ points in Tables 2 and 3 for the non-grey Case $\mathscr{B}$ and Case $\mathscr{C}$, respectively. (The benchmark results for the grey Case $\mathscr{A}$ was given in Ref. [7].) At each time, the results given in the tables can construct reasonably smooth spatial profiles for radiation and material temperature fields. The data given in the tables are accurate at least up to the fourth digit after the decimal point, with the maximum absolute error of order of 10^{-5}. All the data in the tables were generated on a personal workstation and took only few minutes of computational time.

4. Solutions to the transport description

The solutions to the transport equations, given by Eqs. (10) and (11), are obtained by exactly following the approach given earlier for the grey problem [7]. This section is purposely written succinctly, and the reader is referred to Ref. [7] for algebraic details.

4.1. The general solutions

As for the diffusion description, we apply the double transformations, given by Eq. (20), to Eqs. (10) and (11) and obtain

$$(w_n + \varepsilon s + \mathrm{i}\mu k)\,\bar{u}_n(k, \mu, s) = \tfrac{1}{2} p_n w_n \bar{V}(k, s) + \tfrac{1}{2} p_n \bar{Q}(k, s), \tag{57}$$

$$(1 + s)\bar{V}(k, s) = w_1 \bar{U}_1(k, s) + w_2 \bar{U}_2(k, s). \tag{58}$$

In Eq. (58), we have used the relationship between U_n and u_n defined by Eq. (19). Dividing Eq. (57) by $(w_n + \varepsilon s + \mathrm{i}\mu k)$, integrating over μ form -1 to 1, defining

$$r_n(k, s) = \frac{1}{2} \int_{-1}^{1} \frac{\mathrm{d}\mu}{(w_n + \varepsilon s + \mathrm{i}\mu k)}, \tag{59}$$

and using the analogous relationship between $\bar{U}_n$ and $\bar{u}_n$ as Eq. (19), we have the coupled linear algebraic equations for $\bar{U}_n$ and $\bar{V}$. Solving the resultant equations yields

$$\bar{U}_n = p_n r_n \bar{Q} \left[\frac{1 + s - w_m(1 - w_n) r_m}{1 + s - (p_1 w_1^2 r_1 + p_2 w_2^2 r_2)} \right], \quad n, m = 1, 2, m \neq n, \tag{60}$$

$$\bar{V} = \bar{Q} \left[\frac{p_1 w_1 r_1 + p_2 w_2 r_2}{1 + s - (p_1 w_1^2 r_1 + p_2 w_2^2 r_2)} \right]. \tag{61}$$

The transport solutions for $U_n(x, \tau)$ and $V(x, \tau)$ follow from the double Laplace–Fourier inversions of Eqs. (60) and (61). Unfortunately, none of the inversions can be done analytically. As discussed in Ref. [7] for the grey case, all the singularities of $\bar{U}_n$ and $\bar{V}$ are in the left half space of s. Thus, the integration contour of the Laplace inversion is taken as the imaginary axis of s. Setting $s = \mathrm{i}\eta$ and

Table 2
The diffusion benchmarks of $U_1(x, \tau)$, $U_2(x, \tau)$, and $V(x, \tau)$ for Case $\mathscr{B}$

x	$\tau = 0.1$	$\tau = 0.3$	$\tau = 1.0$	$\tau = 3.0$	x	$\tau = 10.0$	x	$\tau = 30.0$
	0.03873[a]	0.08265	0.16857	0.30028		0.54038		0.18634
0.00	0.04578[b]	0.11394	0.23845	0.44678	0.00	0.91470	0.00	0.27740
	0.00452[c]	0.03326	0.20363	0.66656		1.65679		0.55480
	0.03649	0.07923	0.16426	0.29531		0.53144		0.18502
0.20	0.04501	0.10820	0.22479	0.42434	0.25	0.86466	0.50	0.27193
	0.00447	0.03200	0.19265	0.63301		1.56620		0.54352
	0.02951	0.06891	0.15134	0.28045		0.50483		0.18117
0.40	0.03684	0.08416	0.17908	0.35415	0.50	0.71131	1.00	0.25663
	0.00380	0.02552	0.15342	0.52613		1.28823		0.51207
	0.02402	0.06109	0.14164	0.26934		0.46974		0.17510
0.50	0.02293	0.05926	0.14007	0.29871	0.75	0.53047	1.50	0.23431
	0.00229	0.01736	0.11740	0.43986		0.96146		0.46654
	0.01840	0.05282	0.13115	0.25719		0.43543		0.16728
0.60	0.00902	0.03433	0.10051	0.24141	1.00	0.39561	2.00	0.20851
	0.00077	0.00919	0.08102	0.35113		0.71995		0.41440
	0.01027	0.03884	0.11187	0.23393		0.37106		0.14830
0.80	0.00084	0.00994	0.04988	0.15585	1.50	0.22432	3.00	0.15810
	0.00011	0.00258	0.03862	0.22372		0.41695		0.31398
	0.00535	0.02790	0.09478	0.21218		0.26397		0.10764
1.00	0.00004	0.00232	0.02364	0.09963	2.50	0.08847	5.00	0.08984
	0.00003	0.00087	0.01903	0.14403		0.17808		0.17988
	0.00214	0.01785	0.07633	0.18718		0.18465		0.06580
1.25	0.00000	0.00028	0.00882	0.05695	3.50	0.04739	7.50	0.04619
	0.00001	0.00035	0.00882	0.08608		0.10114		0.09326
	0.00075	0.01098	0.06081	0.16454		0.10537		0.03742
1.50	0.00000	0.00003	0.00323	0.03321	5.00	0.02290	10.0	0.02297
	0.00000	0.00018	0.00489	0.05476		0.05035		0.04666
	0.00023	0.00649	0.04793	0.14418		0.05834		0.02006
1.75	0.00000	0.00001	0.00125	0.02023	6.50	0.01118	12.5	0.01089
	0.00000	0.00009	0.00314	0.03754		0.02498		0.02225
		0.00368	0.03735	0.12593		0.03128		0.01021
2.00		0.00000	0.00057	0.01312	8.00	0.00529	15.0	0.00493
		0.00005	0.00218	0.02760		0.01201		0.01014
			0.00650	0.05219		0.01291		0.00496
3.50			0.00004	0.00264	10.0	0.00184	17.5	0.00214
			0.00025	0.00778		0.00429		0.00443
			0.00071	0.01901		0.00389		0.00230
5.00			0.00000	0.00070	12.5	0.00045	20.0	0.00089
			0.00002	0.00228		0.00108		0.00186
				0.00395		0.00105		0.00044
7.00				0.00010	15.0	0.00010	25.0	0.00014
				0.00036		0.00025		0.00029
				0.00062		0.00025		0.00018
9.00				0.00001	17.5	0.00002	27.5	0.00005
				0.00004		0.00005		0.00011

[a]Result for $U_1(x, \tau)$. [b]Result for $U_2(x, \tau)$. [c]Result for $V(x, \tau)$.

Table 3
The diffusion benchmarks of $U_1(x, \tau)$, $U_2(x, \tau)$, and $V(x, \tau)$ for Case $\mathscr{C}$

x	$\tau = 0.1$	$\tau = 0.3$	$\tau = 1.0$	$\tau = 3.0$	x	$\tau = 10.0$	x	$\tau = 30.0$
	0.01828[a]	0.03404	0.06484	0.11433		0.20855		0.06128
0.00	0.04546[b]	0.11251	0.23441	0.44368	0.00	0.93964	0.00	0.35004
	0.00451[c]	0.03340	0.20434	0.67399		1.74573		0.71204
	0.01756	0.03323	0.06397	0.11343		0.20761		0.06123
0.25	0.04411	0.10355	0.21289	0.40645	0.25	0.88173	0.50	0.33536
	0.00444	0.03142	0.18633	0.61576		1.63452		0.68082
	0.01537	0.03079	0.06138	0.11073		0.20482		0.06108
0.50	0.02275	0.05809	0.13483	0.28679	0..50	0.70579	1.00	0.29535
	0.00226	0.01699	0.11294	0.42201		1.29579		0.59613
	0.01263	0.02765	0.05797	0.10717		0.20110		0.06083
0.75	0.00140	0.01247	0.05366	0.15591	0.75	0.49837	1.50	0.24013
	0.00008	0.00254	0.03781	0.21349		0.89912		0.48038
	0.01026	0.02475	0.05470	0.10367		0.19740		0.06013
1.00	0.00002	0.00185	0.01939	0.08076	1.00	0.34348	2.50	0.12910
	0.00001	0.00032	0.01172	0.10346		0.60852		0.25242
	0.00654	0.01959	0.04854	0.09692		0.18296		0.05785
1.50	0.00000	0.00002	0.00191	0.01931	2.00	0.06421	5.00	0.02108
	0.00001	0.00005	0.00118	0.02258		0.10741		0.04111
	0.00396	0.01526	0.04287	0.09047		0.16268		0.05684
2.00	0.00000	0.00000	0.00019	0.00442	3.50	0.00799	6.00	0.01550
	0.00000	0.00004	0.00040	0.00566		0.01577		0.03091
	0.00227	0.01169	0.03770	0.08433		0.14411		0.05529
2.50	0.00000	0.00000	0.00007	0.00137	5.00	0.00505	7.50	0.01319
	0.00000	0.00003	0.00031	0.00256		0.01096		0.02663
	0.00063	0.00652	0.02873	0.07295		0.11678		0.05257
3.50	0.00000	0.00000	0.00005	0.00064	7.50	0.00373	10.0	0.01141
	0.00000	0.00001	0.00022	0.00170		0.00819		0.02309
		0.00237	0.01842	0.05802		0.09361		0.04372
5.00		0.00000	0.00002	0.00045	10.0	0.00275	17.5	0.00735
		0.00000	0.00012	0.00124		0.00608		0.01493
		0.00030	0.00791	0.03838		0.05811		0.03447
7.50		0.00000	0.00001	0.00025	15.0	0.00144	25.0	0.00455
		0.00000	0.00004	0.00072		0.00324		0.00929
			0.00295	0.02435		0.03436		0.02297
10.0			0.00000	0.00013	20.0	0.00072	35.0	0.00225
			0.00001	0.00040		0.00165		0.00463
			0.00026	0.00858		0.01929		0.01025
15.0			0.00000	0.00003	25.0	0.00034	50.0	0.00067
			0.00000	0.00011		0.00080		0.00141
				0.00250		0.00515		0.00359
20.0				0.00001	35.0	0.00007	65.0	0.00017
				0.00003		0.00016		0.00036
				0.00060		0.00046		0.00099
25.0				0.00000	50.0	0.00000	80.0	0.00003
				0.00000		0.00001		0.00007

[a]Result for $U_1(x, \tau)$. [b]Result for $U_2(x, \tau)$. [c]Result for $V(x, \tau)$.

following the procedures given in Ref. [7], we derive a solution representation, which is suitable for numerical evaluation, given by

$$W(x,\tau)=\frac{1}{\pi^2}\int_0^\infty \mathrm{d}k\int_0^\infty \mathrm{d}\eta\,\bar{Q}_1(k)\cos(kx)\times\left[h(k,\eta)\frac{\sin(\eta\tau)-\sin(\eta\tau^*)}{\eta}+q(k,\eta)\frac{\cos(\eta\tau^*)-\cos(\eta\tau)}{\eta}\right]. \tag{62}$$

Equation (62) is a general form for both $U_n(x,\tau)$ and $V(x,\tau)$, and in which we have defined

$$h=\frac{t_1t_3+t_2t_4}{t_1^2+t_2^2}, \tag{63}$$

$$q=\frac{t_2t_3-t_1t_4}{t_1^2+t_2^2}, \tag{64}$$

$$t_1=1-p_1w_1^2g_1-p_2w_2^2g_2, \tag{65}$$

$$t_2=\eta+p_1w_1^2f_1+p_2w_2^2f_2, \tag{66}$$

$$g_n=\frac{1}{2k}\left[\tan^{-1}\left(\frac{k+\varepsilon\eta}{w_n}\right)+\tan^{-1}\left(\frac{k-\varepsilon\eta}{w_n}\right)\right],\quad n=1,2, \tag{67}$$

$$f_n=\frac{1}{2k}\tanh^{-1}\left(\frac{2\varepsilon\eta k}{w_n^2+\varepsilon^2\eta^2+k^2}\right),\quad n=1,2\,. \tag{68}$$

The definitions for t_3 and t_4 depend upon the quantity of interest. For $U_n(x,\tau)$, t_3 and t_4 are given by, with $n,m=1,2$, and $m\neq n$,

$$t_3=p_n[g_n+\eta f_n-w_m(1-w_n)(g_1g_2-f_1f_2)], \tag{69}$$

$$t_4=p_n[\eta g_n-f_n+w_m(1-w_n)(g_1f_2+g_2f_1)]. \tag{70}$$

For $V(x,\tau)$, t_3 and t_4 are given by

$$t_3=p_1w_1g_1+p_2w_2g_2, \tag{71}$$

$$t_4=-(p_1w_1f_1+p_2w_2f_2). \tag{72}$$

Numerical evaluation of Eq. (62), which will be discussed in a later section, produces the benchmark transport results for $U_n(x,\tau)$ and $V(x,\tau)$.

4.2. The asymptotic solutions

The asymptotic analyses for transport solutions also follow the steps given in Ref. [7] for the grey transport description or the steps given in Section 3.2 for the two-group diffusion description. For large times ($\tau\gg\tau_0$), the main contribution to the solutions comes from small s and small k. Thus, we expand all the quantities in $\bar{U}_n$ and $\bar{V}$ at small s and small k, and keep up to the linear terms in s and up to the quadratic terms in k. Specifically, we assume

$$\varepsilon s\ll w_n+\mathrm{i}\mu k,\quad n=1,2 \tag{73}$$

in Eq. (59) for small s and approximate r_n by

$$r_n(k, s) \approx \frac{1}{w_n}\left(1 - \frac{k^2}{3w_n^2}\right) - \frac{\varepsilon s}{w_n^2}\left(1 - \frac{k^2}{w_n^2}\right). \tag{74}$$

We then use this result in Eqs. (60) and (61) and simplify $\bar{U}_n$ and $\bar{V}$ in a similar way as we did in Section 3.2 for the diffusion description. After some algebraic manipulations and the Laplace–Fourier inversions, we find that the asymptotic transport solutions at large times have the same forms as the asymptotic diffusion solutions, i.e., they are given by Eqs. (46) and (47) too. But the parameters β_n and β_v for transport theory are different from those for diffusion theory. For the transport description, β_n and β_v are given by

$$\beta_n = \frac{\alpha_1\tau_0}{2} - (1+\varepsilon)x_0^2 + \varepsilon\alpha_1^2 - \frac{\alpha_1}{w_n} + 3\varepsilon\alpha_2 - (1+\varepsilon)\frac{w_1^2 + w_2^2 - w_n}{w_1^2 w_2^2}, \tag{75}$$

$$\beta_v = \frac{\alpha_1\tau_0}{2} - (1+\varepsilon)x_0^2 + \varepsilon\alpha_1^2 + (2\varepsilon - 1)\alpha_2, \tag{76}$$

where α_1 and α_2 are still defined by Eqs. (50) and (51).

For small τ, the main contribution is due to large s. Therefore, we assume

$$\varepsilon s \gg w_n + \mathrm{i}\mu k, \quad n = 1, 2 \tag{77}$$

in Eq. (59) for large s and approximate r_n by

$$r_n(k, s) \approx \frac{1}{\varepsilon s} - \frac{w_n}{(\varepsilon s)^2} + \frac{w_n^2 - k^2/3}{(\varepsilon s)^3}. \tag{78}$$

We then use this result in $\bar{U}_n$ and $\bar{V}$ and proceed in the same manner as we did in Section 3.2. After the double inversions, the asymptotic transport solutions at small times are found to be identical to the asymptotic diffusion solutions. That is, the asymptotic transport solutions for small τ are also given by Eqs. (53) and (54).

4.3. The numerical results

The numerical evaluation of the general solutions given by Eq. (62) is not exceptionally difficult, although not trivial. The evaluation of the double integrals proceeds in the same manner outlined in an earlier paper [7]. The $\eta - k$ plane is divided into areas whose sides are chosen to be multiples of π. Farther from the origin, as the contribution to the integrals decreases, larger areas are chosen. Each area is evaluated using the multiple integral method discussed in the book *Numerical Recipes in Fortran* [9]. Each one-dimensional integral is evaluated with the open Romberg method to a specified accuracy. However, when the inner one-dimensional integrals are added to compute the two-dimensional integral, the cancellation due to the oscillation of the integrand causes the tolerances for the one-dimensional integrals to be almost useless for quantifying the accuracy of final results. Therefore, we adopt a conservative approach of tightening the error tolerances for the integrals in each area until the final result for U_n and V at each evaluated point is converged to at least 1×10^{-4}. That is, we require as a minimum that the first four digits after the decimal point are converged for each result.

This numerical approach and the algebraic manipulations involved in the derivation of the transport solutions are validated in the exactly same way as we did for diffusion theory. We first perform some calculations for Case $\mathcal{A}$ and find that the numerical results obtained here agree with the grey model results obtained in Ref. [7], as they should. This agreement precludes any doubts associated in algebraic manipulations of deriving Eq. (62). Secondly, the asymptotic transport solutions are compared with the numerical solutions. These results are shown in Fig. 2, with D still defined by Eq. (56). For large times, we see the same phenomenon as in the diffusion description. That is, the agreement between the two solutions deteriorates as the ratio of w_w/w_1 becomes larger and larger. This is also attributed to the fact that the large τ assumption given by Eq. (73) is compromised when w_2/w_1 is large. Because as w_2/w_1 goes to infinity, w_1 goes to zero, which makes Eq. (73) invalid for $n = 1$ and small k. On the other hand, unlike the diffusion results the agreement between asymptotic and numerical transport solutions at small τ seems not affected by the value of w_2/w_1. We attribute this to the fact that the small τ assumption, Eq. (78), is good for any values of w_2/w_1. With the parameters currently used in this work ($p_1 = p_2 = \frac{1}{2}$), w_1 ranges from unity to zero and w_2 ranges from unity to two as w_2/w_1 changes from unity to infinity. In any case, Eq. (78) is a valid assumption for large s. Correspondingly, the small τ asymptotic transport solutions, which are derived based upon Eq. (78), are equally good for any values of w_2/w_1. We note that for very small τ, say for $\tau < 0.1$, the quantity D does not reduce sharply as the decrease of τ. This is caused by the accuracy requirement in our calculation. We require each result to be converged at least to the fourth (fifth in most cases) digit after the decimal point so that the absolute error of each result is small (less than 1×10^{-4}). However, the absolute value of radiation energy density at such small τ is also small (of the order of τ). So the calculated numerical results suffer accuracy loss in relative terms. Anyway, we see from Fig. 2 that the numerical results agree with the asymptotic solutions within reasonably high accuracy in the appropriate ranges and the two solutions converge as τ goes

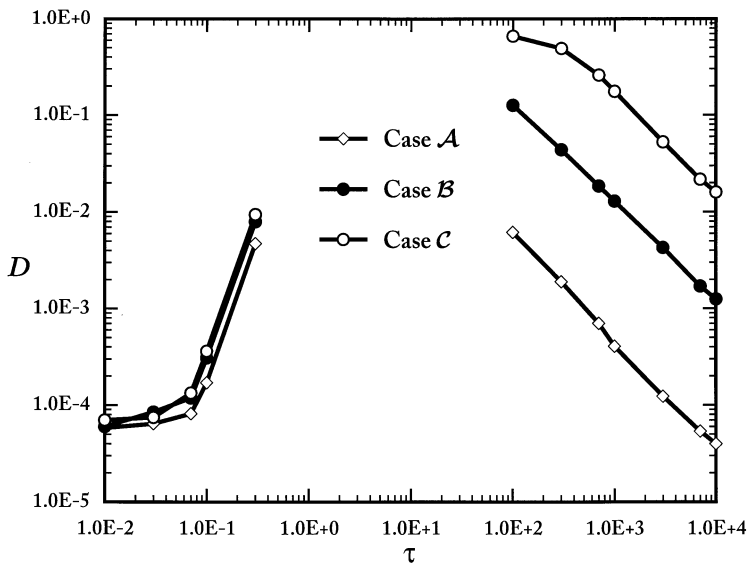

Fig. 2. Comparison between the numerical and asymptotic transport solutions.

to zero or infinity. This comparison proves the correctness of our numerical scheme for the double integrals.

We calculate the benchmarks for the non-grey Cases $\mathscr{B}$ and $\mathscr{C}$ and list the results in Tables 4 and 5, respectively. These results are believed to be accurate at least to the fourth digit after the decimal point. The calculations were performed on a desk-top workstation. For most tabulated points, it only requires seconds or minutes of computation time. However, some points, especially those near the front of wave propagation, have bad sign cancellation and require a large number of integrand evaluations and equivalently much longer computation time to converge.

5. Comparisons between different solutions

Both the diffusion and transport benchmark solutions to the problem have been generated in the two-group picket-fence model in this work, as well as in the one-group grey model in earlier work [7]. For educational purposes, we compare the diffusion solutions with the transport solutions and also compare the picket-fence solutions with the grey solutions in this section. These comparisons are done at time of $\tau = 10$ as an example. Except at very large times ($\tau \gg \tau_0$) where the asymptotic solutions apply, the comparisons between solutions at other times are quite similar to those at $\tau = 10$. Therefore, conclusions drawn from the comparisons at $\tau = 10$ are exemplary.

5.1. Diffusion theory versus transport theory

In order to visualize the numerical results and difference between the transport solutions and the diffusion ones, we show in Fig. 3 the diffusion and transport radiation energy density profiles at $\tau = 10$ for the three cases we considered in the previous sections. The quantity shown in the figure is the total radiation energy density U, which equals to $U_1 + U_2$ for Cases $\mathscr{B}$ and $\mathscr{C}$. The results for Case $\mathscr{A}$ are either taken from Ref. [7] or are calculated from the picket-fence model. Clearly, the difference between transport and diffusion theories is significant and such difference depends upon the opacity ratio w_2/w_1. For the grey Case $\mathscr{A}$ ($w_2/w_1 = 1$), diffusion theory approximates transport theory reasonably well. Diffusion theory predicts results about 17% lower than the correct transport theory results near $x = 0$; and allows radiation to propagate only a little faster than transport theory. However, as w_2/w_1 becomes larger and larger, diffusion theory performs more-and-more poorly. For Case $\mathscr{B}$, whose w_2/w_1 is 10, diffusion theory underestimates the total radiation energy density near $x = 0$ by 30% and it predicts radiation propagating significantly (about 2 times) faster than that of transport theory. For Case $\mathscr{C}$ with $w_2/w_1 = 100$, the situation is even more worse: diffusion theory predicts the total radiation energy density at $x = 0$ about 45% lower than the correct one and allows radiation to propagate into the medium far ahead of transport theory (about 4 times further). For this case, the diffusion solution for the total radiation energy density clearly suggests that there are two distinguishable groups of radiation traveling at different speeds; and one group (U_1) travels much much faster than the other (U_2). The transport solution for the total radiation energy density does not show this type of structure.

Diffusion theory not only predicts quantitatively inaccurate solutions, but may also predicts qualitatively incorrect results. In Fig. 4, we plot the ratio of the material energy density V to the radiation energy density U as a function of x for all the diffusion and transport solutions at $\tau = 10$.

Table 4
The transport benchmarks of $U_1(x, \tau)$, $U_2(x, \tau)$, and $V(x, \tau)$ for Case $\mathscr{B}$

x	$\tau = 0.1$	$\tau = 0.3$	$\tau = 1.0$	$\tau = 3.0$	x	$\tau = 10.0$	x	$\tau = 30.0$
	0.04956[a]	0.14632	0.39890	0.65095		0.99191		0.23014
0.00	0.04585[b]	0.11858	0.26676	0.51786	0.00	1.09334	0.00	0.32932
	0.00458[c]	0.03511	0.23884	0.81005		2.04024		0.66113
	0.04956	0.14632	0.39418	0.64570		0.98586		0.22899
0.10	0.04585	0.11858	0.26401	0.51216	0.10	1.08380	0.30	0.32625
	0.00458	0.03511	0.23680	0.80144		2.02233		0.65473
	0.04956	0.14181	0.35349	0.60076		0.93473		0.22319
0.30	0.04585	0.11563	0.23839	0.46275	0.30	1.00449	0.75	0.31066
	0.00458	0.03489	0.21640	0.72556		1.87299		0.62278
	0.04578	0.10753	0.28118	0.52264		0.79425		0.21808
0.45	0.04254	0.08956	0.18496	0.37580	0.50	0.80678	1.00	0.29773
	0.00446	0.02893	0.16752	0.58601		1.49569		0.59549
	0.02478	0.07316	0.23277	0.47187		0.61503		0.20912
0.50	0.02293	0.05929	0.14353	0.32037	0.75	0.55166	1.35	0.27532
	0.00229	0.01756	0.12369	0.49152		1.01212		0.54935
	0.00378	0.03879	0.18410	0.42049		0.51225		0.19533
0.55	0.00331	0.02902	0.10206	0.26455	1.00	0.39861	1.80	0.24272
	0.00012	0.00617	0.07986	0.39651		0.72941		0.48282
		0.00105	0.09013	0.31167		0.40883		0.17668
0.75		0.00066	0.03736	0.15017	1.35	0.25760	2.35	0.20221
		0.00002	0.02270	0.21608		0.47338		0.40111
			0.03332	0.22950		0.31043		0.14935
1.00			0.01016	0.07857	1.80	0.15077	3.15	0.15049
			0.00427	0.11109		0.28209		0.29821
			0.00250	0.15410		0.23303		0.11748
1.35			0.00054	0.03199	2.35	0.08256	4.20	0.10164
			0.00007	0.04604		0.16026		0.20216
				0.09082		0.15545		0.08451
1.80				0.00963	3.15	0.03885	5.60	0.06293
				0.01513		0.08031		0.12619
				0.04035		0.09376		0.05392
2.35				0.00182	4.20	0.01707	7.50	0.03517
				0.00336		0.03767		0.07113
				0.00316		0.04773		0.02967
3.15				0.00004	5.60	0.00611	10.0	0.01696
				0.00007		0.01441		0.03455
						0.01691		0.01265
					7.50	0.00113	13.5	0.00601
						0.00305		0.01238
						0.00494		0.00423
					9.00	0.00011	18.0	0.00140
						0.00041		0.00297
						0.00053		0.00080
					10.0	0.00000	23.5	0.00013
						0.00000		0.00030

[a]Result for $U_1(x, \tau)$. [b]Result for $U_2(x, \tau)$. [c]Result for $V(x, \tau)$.

Table 5
The transport benchmarks of $U_1(x,\tau)$, $U_2(x,\tau)$, and $V(x,\tau)$ for Case $\mathscr{C}$

x	$\tau = 0.1$	$\tau = 0.3$	$\tau = 1.0$	$\tau = 3.0$	x	$\tau = 10.0$	x	$\tau = 30.0$
	0.04995[a]	0.14959	0.42044	0.69138		0.99007		0.11347
0.00	0.04551[b]	0.11622	0.25595	0.48965	0.00	1.05000	0.00	0.39038
	0.00454[c]	0.03419	0.22354	0.74944		1.96476		0.79478
	0.04995	0.14959	0.41545	0.68633		0.98490		0.11187
0.10	0.04551	0.11622	0.25339	0.48413	0.10	1.03985	0.75	0.35243
	0.00454	0.03419	0.22177	0.74128		1.94533		0.71378
	0.04995	0.14489	0.37258	0.64299		0.94074		0.10873
0.30	0.04551	0.11340	0.22925	0.43605	0.30	0.95569	1.35	0.28293
	0.00454	0.03398	0.20359	0.66860		1.78386		0.56724
	0.04612	0.10963	0.29748	0.56722		0.81370		0.10577
0.45	0.04224	0.08801	0.17768	0.35043	0.50	0.74874	1.80	0.22416
	0.00442	0.02828	0.15772	0.53231		1.38266		0.44522
	0.02498	0.07480	0.24799	0.51747		0.65444		0.10197
0.50	0.02275	0.05811	0.13694	0.29537	0.75	0.48244	2.35	0.15860
	0.00227	0.01709	0.11507	0.43873		0.87032		0.31139
	0.00383	0.03996	0.19819	0.46710		0.56954		0.09679
0.55	0.00327	0.02820	0.09615	0.23998	1.00	0.32429	3.15	0.08941
	0.00012	0.00591	0.07242	0.34474		0.57474		0.17339
		0.00110	0.09961	0.36071		0.48630		0.09128
0.75		0.00063	0.03403	0.12874	1.35	0.18484	4.20	0.04321
		0.00002	0.01913	0.17138		0.32123		0.08386
			0.03777	0.27848		0.40928		0.08591
1.00			0.00896	0.06243	1.80	0.08860	5.60	0.02280
			0.00330	0.07746		0.15199		0.04531
			0.00291	0.19880		0.33982		0.08076
1.35			0.00046	0.02259	2.35	0.03664	7.50	0.01545
			0.00005	0.02595		0.06370		0.03126
				0.12568		0.26564		0.07586
1.80				0.00580	3.15	0.01204	10.0	0.01105
				0.00625		0.02290		0.02251
				0.05994		0.19510		0.07089
2.35				0.00094	4.20	0.00457	13.5	0.00695
				0.00098		0.00994		0.01432
				0.00502		0.12713		0.06641
3.15				0.00002	5.60	0.00188	18.0	0.00338
				0.00000		0.00448		0.00718
						0.06122		0.03698
					7.50	0.00045	23.5	0.00077
						0.00123		0.00176
						0.02201		0.01515
					9.00	0.00000	27.0	0.00013
						0.00020		0.00034
						0.00262		0.00475
					10.0	0.00000	29.0	0.00001
						0.00000		0.00004

[a]Result for $U_1(x,\tau)$. [b]Result for $U_2(x,\tau)$. [c]Result for $V(x,\tau)$.

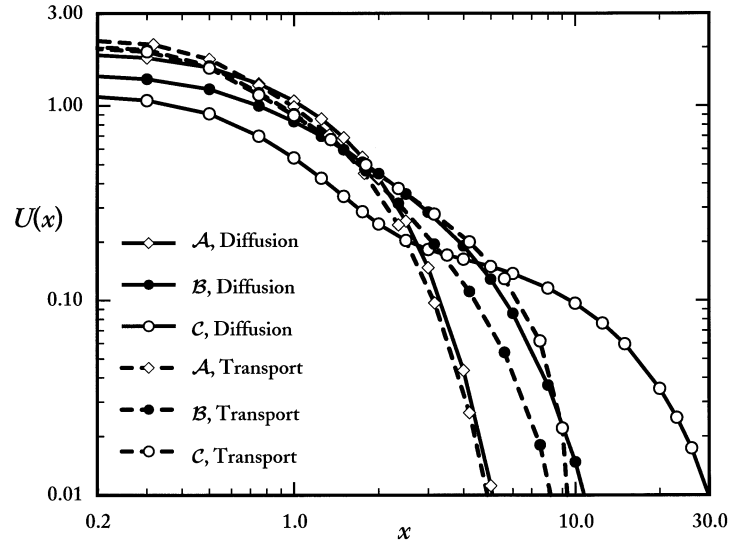

Fig. 3. Comparison between diffusion and transport solutions for radiation energy density at $\tau = 10$.

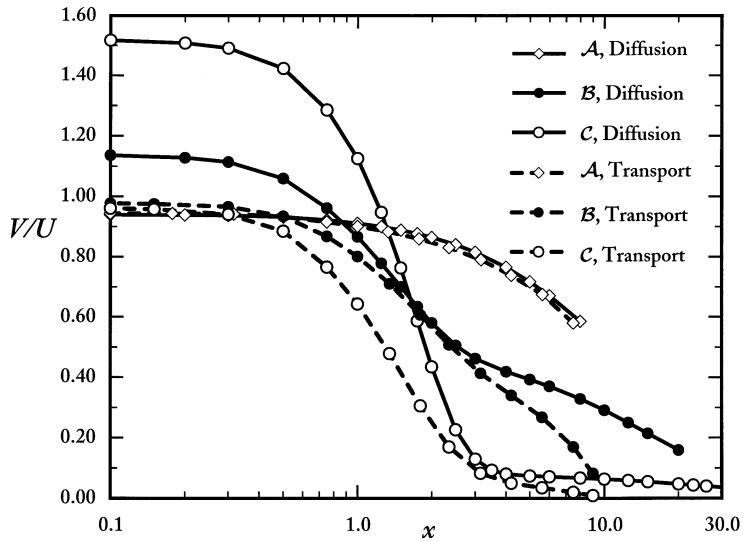

Fig. 4. Comparison between diffusion and transport results for the ratio of material energy density to radiation energy density at $\tau = 10$.

The transport solutions show that V/U is below unity everywhere for all the three cases. This is a physically correct phenomenon. Because when the radiation source is on, it is the radiation that heats up material so that the material temperature field V should lag behind of the radiation field U, i.e. $V < U$. However, the diffusion description predicts contrary results ($V/U > 1$) and tells that

the radiation field U lags behind the material temperature field V in and near the source region for Cases $\mathscr{B}$ and $\mathscr{C}$. The reason for this non-physical behavior is as follows. Compared with the transport results, diffusion theory underestimates both U and V for small x. But the underestimation is more severe for U than V. It underestimates U in source region by about 30% and 45%, respectively; and only underestimates V by about 18 and 11%, respectively, for Case $\mathscr{B}$ and Case $\mathscr{C}$. Since the transport results for U and V are very close to each other in the source region, diffusion theory correspondingly ends up with predicting a larger value for V than U for small x.

From these comparisons, we see that diffusion theory performs poorly for Cases $\mathscr{B}$ and $\mathscr{C}$ and should not be used to approximate the picket-fence transport model when the opacity ratio w_2/w_1 is large. Perhaps this conclusion should be expected *a priori*. Because as w_2/w_1 becomes large, w_1 is small and equivalently the problem is optically thin for the first radiation group $U_1(x, \tau)$. Diffusion theory cannot work well for optically thin problems.

5.2. The picket-fence model versus the grey model

We now compare the two-group picket-fence solutions with corresponding grey solutions. In radiative transfer, there are two commonly used approaches to define a mean opacity for the grey model, namely the Planck mean and the Rosseland mean. For the picket-fence model of $\kappa(v)$ we are considering in this work, the Planck mean opacity is given by

$$\kappa_{\mathrm{P}} = p_1\kappa_1 + p_2\kappa_2 \tag{79}$$

and the Rosseland mean opacity is given by

$$\frac{1}{\kappa_{\mathrm{R}}} = \frac{p_1}{\kappa_1} + \frac{p_2}{\kappa_2}. \tag{80}$$

We see that the Planck mean is simply the averaged opacity defined earlier by Eq. (4). If we set $\bar{\kappa} = 1$ for the problem, then Cases $\mathscr{B}$ and $\mathscr{C}$ have the same Planck mean, i.e. $\kappa_{\mathrm{P}} = 1$. Hence the Planck mean grey solutions for both Cases $\mathscr{B}$ and $\mathscr{C}$ are the same and equal to the solutions of Case $\mathscr{A}$. On the other hand, the Rosseland means for Cases $\mathscr{B}$ and $\mathscr{C}$ are different. By the definition we have $\kappa_{\mathrm{R}} = \frac{40}{121}$ for Case $\mathscr{B}$ and $\kappa_{\mathrm{R}} = \frac{400}{10\,201}$ for Case $\mathscr{C}$, again under the condition of $\bar{\kappa} = 1$. Scaling the spatial and temporal variables (x and τ) as well as the source parameters (x_0 and τ_0) by κ_{R}, we can compute the Rosseland mean grey solutions for Cases $\mathscr{B}$ and $\mathscr{C}$ by using the numerical schemes developed in this work for Case $\mathscr{A}$ or those developed in Ref. [7].

The comparisons between the two-group solutions, the Planck-mean grey solutions, and the Rosseland-mean grey solutions are presented for Cases $\mathscr{B}$ and $\mathscr{C}$ in Figs. 5–8. These comparisons are made at $\tau = 10$ and for the total radiation energy density U and the material energy density V. The results of diffusion theory are given in Figs. 5 and 6 for U and V, respectively; and the results of transport theory are given in Figs. 7 and 8 for U and V, respectively. These figures are quite self-explanatory. Nevertheless, we summarize some general trends as follows. First of all, it is more feasible to approximate the picket-fence model by a grey model for transport theory than for diffusion theory. These figures clearly show that the grey models in the transport description do a better job than their counterparts in the diffusion description. The differences between the two-group solutions and one-group solutions are consistently smaller in transport theory than those in diffusion theory. Secondly, when the ratio w_2/w_1 is not too large (like Case $\mathscr{B}$), the use of

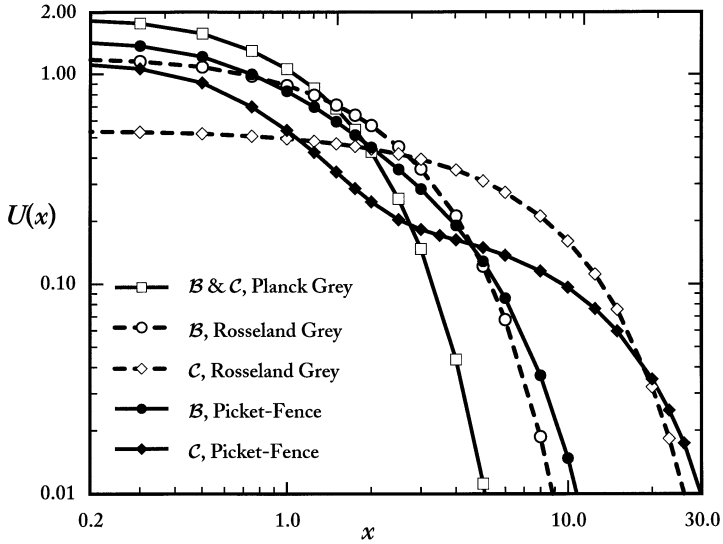

Fig. 5. Comparison between grey and non-grey diffusion solutions for radiation energy density at $\tau = 10$.

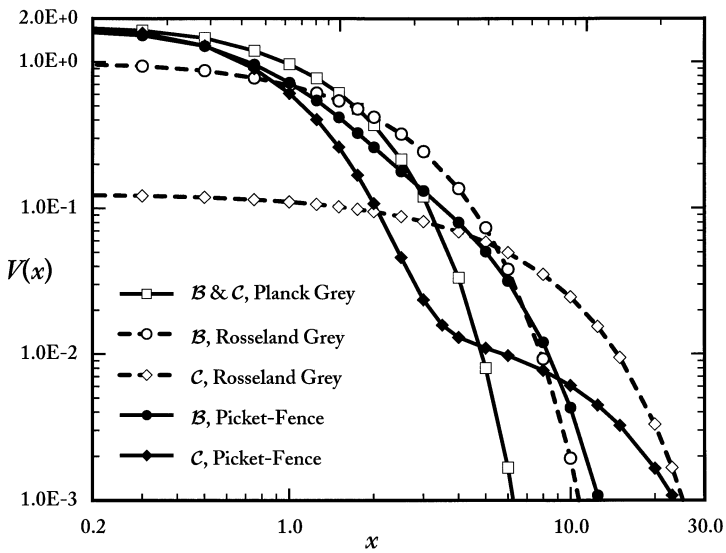

Fig. 6. Comparison between grey and non-grey diffusion solutions for material energy density at $\tau = 10$.

the Rosseland mean is, in general, superior to the use of the Planck mean in both diffusion and transport theories, even though either could result in significant errors. This is consistent with other similar observations in the literature. Thirdly, when the ratio w_2/w_1 is very large (like Case $\mathscr{C}$), neither of the grey models works. They both produce poor results. However, it seems that the Planck mean predicts better results near $x = 0$ than the Rosseland mean; and the Rosseland mean

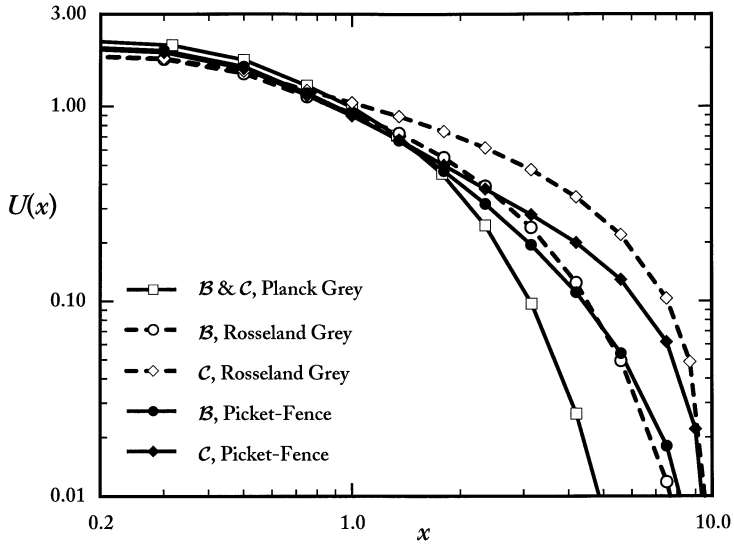

Fig. 7. Comparison between grey and non-grey transport solutions for radiation energy density at $\tau = 10$.

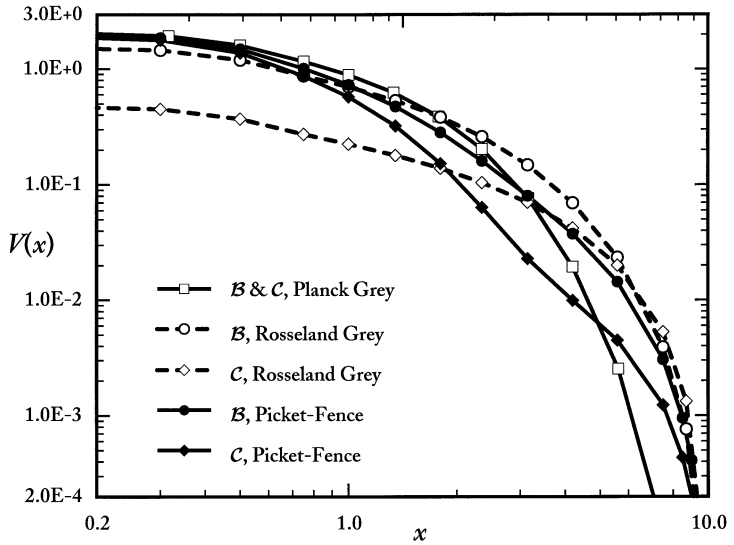

Fig. 8. Comparison between grey and non-grey transport solutions for material energy density at $\tau = 10$.

predicts better results near the wave front than the Planck mean in both theories. Finally, we see that the Planck mean predicts more accurate results for V than U near $x = 0$; on the contrary, the Rosseland mean yields more accurate results for U than V near $x = 0$. The comparisons given here may not be typical for other radiative transfer problems. However, it is interesting to notice these differences.

6. Concluding remark

To include the frequency variable, we have considered a non-equilibrium radiative transfer problem in an infinite medium by using the two-group picket-fence model in this work. The full space-time solutions to this problem are constructed in both diffusion and transport theory. We have also derived the asymptotic small-time and large-time solutions in terms of elementary functions. These asymptotic solutions are used to validate the numerical schemes for generating numerical solutions. Very accurate benchmark results are given in this paper. To the best of our knowledge, this may be the first two-group, analytical solutions for a two-temperature non-equilibrium radiative transfer problem. We hope the data given here will be useful in code development for multigroup time-dependent radiation transport.

Comparisons between different solutions reveal that when the ratio of opacity w_2/w_1 is large, the diffusion description is not a valid approximation to the transport description and may predict non-physical results. These comparisons also confirm the notion that the use of the Rosseland mean is, in general, superior to the use of the Planck mean for small and moderate values of w_2/w_1.

Acknowledgements

The work was performed under the auspices of the U.S. Department of Energy. The first author acknowledges that part of his work was performed at Los Alamos National Laboratory under an appointment of the Director's Fellowship.

References

[1] Marshak RE. Effect of radiation on shock wave behavior. Phys Fluids 1958;1:24–29.
[2] Pomraning GC. The non-equilibrium Marshak wave problem. JQSRT 1979;21:249–261.
[3] Shokair IR, Pomraning GC. Boundary conditions for differential approximations. JQSRT 1981;25:325–337.
[4] Su B, Olson GL. Benchmark results for the non-equilibrium Marshak diffusion problem. JQSRT 1996;56:337–351.
[5] Ganapol BD, Pomraning GC. The non-equilibrium Marshak wave problem: a transport theory solution. JQSRT 1983;29:311–320.
[6] Ganapol BD. The non-equilibrium Marshak wave problem: a radiative transfer benchmark. Unpublished technical report, Los Alamos National Laboratory, Los Alamos, New Mexico, 1986.
[7] Su B, Olson GL. An analytical benchmark for non-equilibrium radiative transfer in an isotropically scattering medium. Ann Nuclear Energy 1997;24:1035–1055.
[8] Råde L, Westergren B. BETA — Mathematics Handbook. Studentlitteratur, Sweden, 1992, pp. 63–64.
[9] Press WH, Teukolsky SA, Vetterling WT, Flannery BP. Numerical Recipes in Fortran, 2nd edn. Cambridge Univ. Press, New York, 1992, pp. 155–158.